(Read at the Spring Meeting of The Society of Naval Architects of Japan, May 1985)

Calculation of Ship Viscous Resistance and Its Application

by Tetsuo Nagamatsu*, *Member*

Summary

The present paper describes a method for calculating viscous resistance of ships based on a higher order boundary layer theory, which is solved by the integral method. Higher order terms in the direction normal to the hull surface were thoroughly examined on the basis of the flow characteristics measured near the stern for an 8 meter long ship model. Viscous-inviscid interaction is taken into account by an iterative calculation procedure with underrelaxation method. The frictional and viscous pressure resistance components are calculated separately by integrating wall shear stress and pressure over the hull surface to obtain explicitly the correlation between hull form and viscous resistance components. Furthermore, in order to change the ship hull form systematically and easily, the ship form is represented by use of the exponential splines.

From comparison between calculations and measurements, it is found that the present method predicts the viscous resistance of full form ships with allowable accuracy and will become a useful tool for systematic investigations of various ship forms in the course of hull form design.

1. Introduction

It is the recent trend in the hull form development that means based on towing tank testings are complemented by advanced hydrodynamic theories. Determining a ship hull form with low viscous resistance is one of the important technical items in the design of full hull form. To obtain viscous resistance theoretically, calculation of viscous flow around ship hull is necessary, and there are two methods available nowadays. One is the integral method and the other the differential one. The latter has high potential to predict complicated turbulent stern flow with three-dimensional separation, which is very difficult to predict by the former method. From the aspects of cost and easiness to use, however, the integral method is advantageous for routine use, especially when use is made for a large number of iteration such as optimization procedure.[1] The method is also effective to formulate the correlation between ship hull form and its viscous resistance explicitly.

In the author's previous paper[2], the integral method was adopted to solve higher order boundary layer equations taking into account pressure variation across the boundary layer and viscous-inviscid interaction, and ship viscous resistance was calculated as a sum of frictional and viscous pressure resistance obtained by integrating wall shear stress and pressure over the hull surface respectively. This method for calculating viscous resistance is useful to know directly the contribution of local ship form to each component of viscous resistance as compared with a method using Squire-Young formula, which estimates only total viscous resistance.

The method described in the present paper is a result of some improvements over the author's previous method.

(1) The variation of metrics and curvatures in the direction normal to the hull surface is taken into account.

(2) All convective terms in the direction normal to the hull surface are taken into account on the basis of the flow characteristics measured near the stern.

(3) For faster convergence in numerical calculation, an iterative procedure with underrelaxation for viscous-inviscid interaction is adopted.

(4) Viscous pressure resistance component produced at the region downstream of numerical breakdown is estimated by referring to the pressure measurement close to the stern end.

* Nagasaki Experimental Tank, Mitsubishi Heavy Industries, Ltd.

Furthermore, for the handy use of the present computational method in hull form design, the ship form is represented by use of exponential splines which is simple and improves the degree of fitting of hull forms.

Lastly, some calculated examples are shown and the applicability of the present method for design purpose is discussed.

2. Governing Equations for Thick Boundary Layer Near the Stern

2.1 Higher order boundary layer equations

From many experiments and calculations made in the last decade, it is found that the ordinary first order boundary layer equations can be applicable to the flow over a large part of a ship hull, but not to the flow close to the ship stern, where the boundary layer thickness is non-uniform along frameline. The boundary layer is thin at the bottom due to the extreme divergence of streamlines and thick at the side, especially at a concave part of frameline near a half of drauhgt, due to convergence of streamlines in addition to the decrease of the body sectional area. Such thick boundary layer is characterized by, for instance, strong viscous-inviscid interaction, pressure variation across the boundary layer, lower turbulence level than that in thin boundary layer and noticeable magnitude of normal velocity component. On the other hand, it is well known that viscous pressure resistance is closely connected to the shape of ship stern. Therefore, instead of the ordinary boundary layer equations, higher order boundary layer equations including above characteristics of the thick boundary layer should be derived to calculate viscous pressure resistance.

Streamline coordinate system (ξ, η, ζ) shown in Fig. 1 is adopted in the present study. ξ-axis coincides with the projection of inviscid streamlines just outside the boundary layer to the ship hull surface, and η-axis intersects orthogonally to the ξ-axis on the hull surface. ζ-axis is outward normal to the hull surface. h_1, h_2 and h_3 are metric coefficients of the streamline coordinates. If h_3 is assumed from the boundary layer approximation to be unity, h_1 and h_2 at an arbitrary position in space can be expressed as

$$h_1=h_{1w}(1+K_{13w}\zeta)\,,\quad h_2=h_{2w}(1+K_{23w}\zeta) \tag{1}$$

where subscript w means the value at the wall. K_{13} and K_{23} are normal curvatures and defined as[3]

$$K_{13}=\frac{K_{13w}}{1+K_{13w}\zeta}\,,\quad K_{23}=\frac{K_{23w}}{1+K_{23w}\zeta} \tag{2}$$

$$K_{13w}=\frac{1}{h_{1w}}\left(\frac{\partial h_1}{\partial\zeta}\right)_w\,,\quad K_{23w}=\frac{1}{h_{2w}}\left(\frac{\partial h_2}{\partial\zeta}\right)_w \tag{3}$$

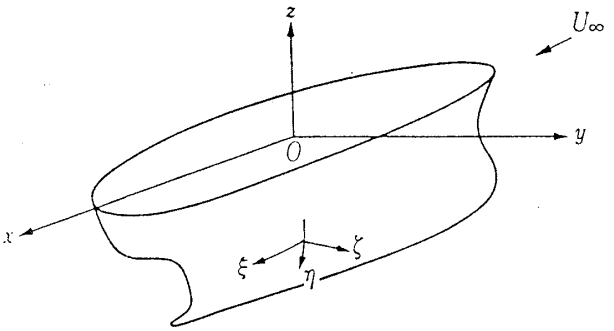

Fig. 1 Coordinate system

Geodesic curvatures K_{21} and K_{12} are also defined as

$$\left.\begin{aligned}K_{21}&=\frac{K_{21w}}{1+K_{13w}\zeta}+\frac{\zeta}{(1+K_{13w}\zeta)(1+K_{23w}\zeta)}\\&\quad\times\frac{\partial K_{23w}}{h_{1w}\partial\xi}\\K_{12}&=\frac{K_{12w}}{1+K_{23w}\zeta}+\frac{\zeta}{(1+K_{13w}\zeta)(1+K_{23w}\zeta)}\\&\quad\times\frac{\partial K_{13w}}{h_{2w}\partial\eta}\end{aligned}\right\} \tag{4}$$

where

$$K_{21w}=\frac{1}{h_{1w}h_{2w}}\frac{\partial h_{2w}}{\partial\xi}\,,\quad K_{12w}=\frac{1}{h_{1w}h_{2w}}\frac{\partial h_{1w}}{\partial\eta} \tag{5}$$

Normal curvatures, which are not considered in the ordinary boundary layer equations, play an important role on characterizing the pressure variation across the boundary layer and turbulent shear stresses in the stern flow, so that the terms of normal curvatures should be retained in the governing equations. Thus, higher order boundary layer equations applicable to the thick boundary layer near the stern are derived as

$$\begin{aligned}&\frac{u}{h_1}\frac{\partial u}{\partial\xi}+\frac{v}{h_2}\frac{\partial u}{\partial\eta}+w\frac{\partial u}{\partial\zeta}+(K_{12}u-K_{21}v)v\\&\quad+K_{13}uw+\frac{1}{h_1}\frac{\partial}{\partial\xi}\left(\frac{p}{\rho}\right)-\frac{1}{\rho}\frac{\partial\tau_{13}}{\partial\zeta}\\&\quad-(2K_{13}+K_{23})\frac{\tau_{13}}{\rho}=0\end{aligned} \tag{6}$$

$$\begin{aligned}&\frac{u}{h_1}\frac{\partial v}{\partial\xi}+\frac{v}{h_2}\frac{\partial v}{\partial\eta}+w\frac{\partial v}{\partial\zeta}+K_{23}vw\\&\quad+(K_{21}v-K_{12}u)u+\frac{1}{h_2}\frac{\partial}{\partial\eta}\left(\frac{p}{\rho}\right)\\&\quad-\frac{1}{\rho}\frac{\partial\tau_{23}}{\partial\zeta}-(2K_{23}+K_{13})\frac{\tau_{23}}{\rho}=0\end{aligned} \tag{7}$$

$$\begin{aligned}&\frac{u}{h_1}\frac{\partial w}{\partial\xi}+\frac{v}{h_2}\frac{\partial w}{\partial\eta}+w\frac{\partial w}{\partial\zeta}-K_{13}u^2\\&\quad-K_{23}v^2+\frac{\partial}{\partial\zeta}\left(\frac{p}{\rho}\right)=0\end{aligned} \tag{8}$$

and the continuity equation becomes

$$\frac{1}{h_1}\frac{\partial u}{\partial \xi}+\frac{1}{h_2}\frac{\partial v}{\partial \eta}+\frac{\partial w}{\partial \zeta}+K_{21}u+K_{12}v+(K_{13}+K_{23})w=0 \qquad (9)$$

where τ_{13} and τ_{23} are the shear stress components including Reynolds stresses. These equations are identical with those in the previous paper[2] except the first three terms in Eq. (8). Eq. (8) describes the pressure variation across the boundary layer and then closely relates to the viscous pressure resistance. It is therefore important to evaluate the order of magnitude of each term of Eq. (8) precisely based on the experimental investigation.

2.2 Experimental evaluation of higher order terms

For the purpose to examine the order of magnitude of each term of Eq. (8), flow measurements were carried out along potential streamlines calculated by Hess-Smith method near the stern of a full form ship model, Ship-A, as shown in Fig. 2. The ship model is geometrically similar to the model used in research program SR107[4]. The length between perpendiculars is 8.0 m and the block coefficient 0.83. A five-hole probe of NPL type of 3 mm in diameter was used for the measurements of velocity components and pressure. The probe was traversed in the direction normal to the hull surface. The spatial deriva-

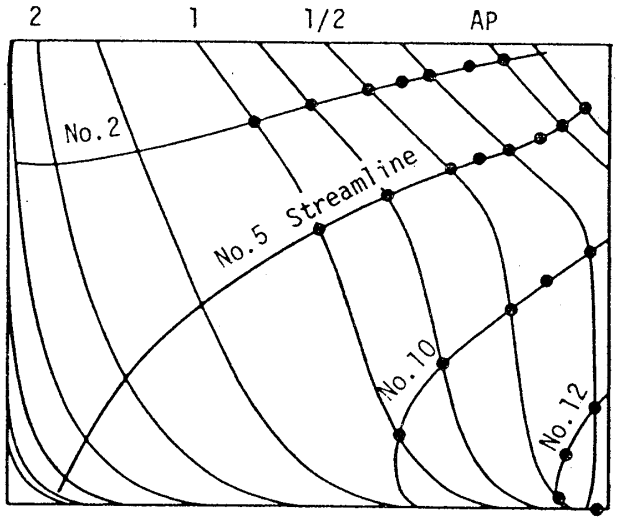

Fig. 2 After-body plan and streamlines of Ship-A

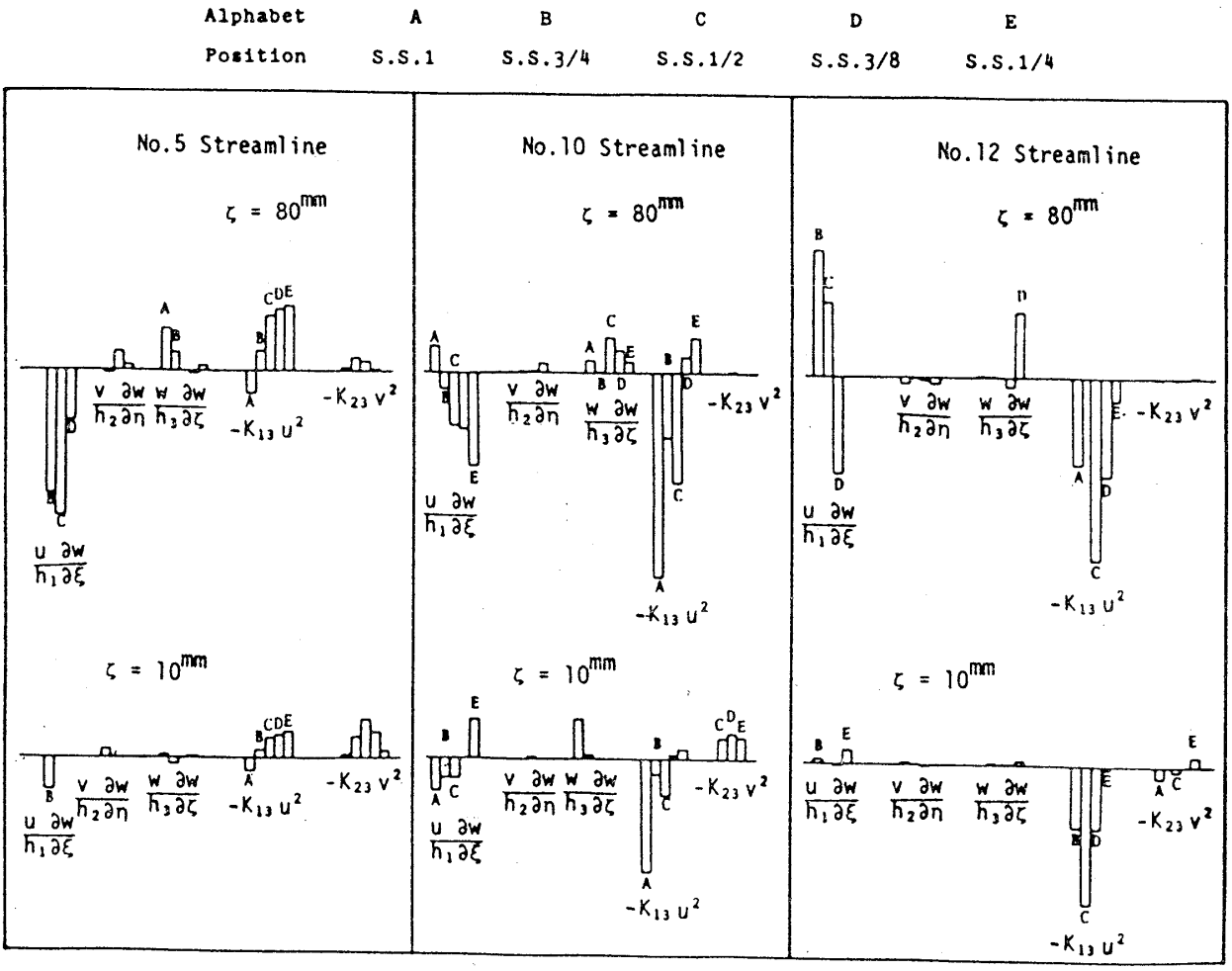

Fig. 3 Comparison of magnitude of higher order terms in Eq. (8)

tives of velocity components were obtained from the gradient of the curves fitted to the measured values and then each term of Eq. (8) was evaluated. Some examples are shown in Fig. 3. The values of the normal curvatures K_{13w} and K_{23w} calculated on the body surface were used here.

The measuring points are not so dense to evaluate precisely the velocity gradients included in Eq. (8), so that the diagrams in Fig. 3 are not fully valid quantitatively but may be sufficient to compare the order of magnitude of the each term qualitatively. It is found that the fourth term in Eq. (8) is the most dominant term. The first three terms in Eq. (8) are as same as or larger rather than the fifth term. From this fact, all terms in Eq. (8) are retained in the present study, while the present author dropped the first three terms in the previous paper[2], and Larsson and Chang dropped the second and the fifth terms under the small cross flow assumption[5].

2.3 Equations for boundary layer calculation

In the present paper, the integral method is adopted to solve the aforementioned governing equations. The momentum integral equations based on the streamline coordinate system are derived from the similar manner to the previous paper and are written as

$$\begin{aligned}&\frac{1}{h_{1w}}\frac{\partial\bar{\theta}_{11}}{\partial\xi}+\left\{2\bar{\theta}_{11}+\bar{\delta}_1^*+2(K_{13w}\bar{I}_1+K_{23w}\bar{I}_2-\bar{I}_3)\right\}\\&\quad\times\frac{1}{U}\frac{\partial U}{h_{1w}\partial\xi}+\frac{1}{h_{2w}}\frac{\partial\bar{\theta}_{12}}{\partial\eta}+(\bar{\theta}_{12}+\bar{\theta}_{21})\\&\quad\times\left(\frac{1}{U}\frac{\partial U}{h_{2w}\partial\eta}+K_{12w}\right)+K_{21w}(\bar{\theta}_{11}-\bar{\theta}_{22})\\&\quad+K_{13w}\left(\bar{\theta}_{31}+\frac{w}{U}\bar{\delta}_1^*\right)+\frac{1}{h_{1w}}\frac{\partial}{\partial\xi}\\&\quad\times\{K_{13w}\bar{I}_1+K_{23w}\bar{I}_2-\bar{I}_3\}+\hat{\theta}_{21}\frac{\partial K_{13w}}{h_{2w}\partial\eta}\\&\quad-(\hat{\theta}_{22}+K_{13w}\hat{I}_1+K_{23w}\hat{I}_2-\hat{I}_3)\frac{\partial K_{23w}}{h_{1w}\partial\xi}\\&=\frac{\tau_{13w}}{\rho U^2}-K_{13w}\bar{T}_1\end{aligned}\tag{10}$$

$$\begin{aligned}&\frac{1}{h_{1w}}\frac{\partial\bar{\theta}_{21}}{\partial\xi}+\frac{2\bar{\theta}_{21}}{U}\frac{\partial U}{h_{1w}\partial\xi}+\frac{1}{h_{2w}}\frac{\partial\bar{\theta}_{22}}{\partial\eta}\\&\quad+\frac{2}{U}\{\bar{\theta}_{22}+K_{13w}\bar{I}_1+K_{23w}\bar{I}_2-\bar{I}_3\}\frac{\partial U}{h_{2w}\partial\eta}\\&\quad+2K_{21w}\bar{\theta}_{21}+K_{12w}(\bar{\theta}_{22}-\bar{\theta}_{11}-\bar{\delta}_1^*)+K_{23w}\bar{\theta}_{23}\\&\quad+\frac{1}{h_{2w}}\frac{\partial}{\partial\eta}\{K_{13w}\bar{I}_1+K_{23w}\bar{I}_2-\bar{I}_3\}\\&\quad-\left\{\hat{\theta}_{11}+\hat{\delta}_1^*-\frac{\hat{\delta}}{1+K_{13w}\delta}+K_{13w}\hat{I}_1+K_{23w}\hat{I}_2\right.\\&\quad\left.-\hat{I}_3\right\}\frac{\partial K_{13w}}{h_{2w}\partial\eta}=\frac{\tau_{23w}}{\rho U^2}-K_{23w}\bar{T}_2\end{aligned}\tag{11}$$

where the integral parameters are defined in Appendix.

The Coles' wall-wake law is used as the velocity profile in the boundary layer

$$\left.\begin{aligned}u&=u_*f_0\left(\frac{u_*\zeta}{\nu}\right)\cos\beta+Uk_1f_1(\zeta/\delta)\\v&=u_*f_0\left(\frac{u_*\zeta}{\nu}\right)\sin\beta+Uk_2f_1(\zeta/\delta)\end{aligned}\right\}\tag{12}$$

where

$$\left.\begin{aligned}f_0\left(\frac{u_*\zeta}{\nu}\right)&=\frac{1}{\kappa}\ln\left(\frac{u_*\zeta}{\nu}\right)+B\\f_1(\zeta/\delta)&=\frac{1}{2}\left\{1-\cos\left(\frac{\pi\zeta}{\delta}\right)\right\}\end{aligned}\right\}\tag{13}$$

and

$$\kappa=0.41,\quad B=0.50\tag{14}$$

β and u_* are wall cross flow angle and friction velocity respectively and defined by

$$\tan\beta=\frac{\tau_{23w}}{\tau_{13w}}\tag{15}$$

$$u_*=\sqrt{\tau_w/\rho}\ ,\quad \tau_w^2=\tau_{13w}^2+\tau_{23w}^2\tag{16}$$

k_1 and k_2 are obtained by substituting $\zeta=\delta$ into Eq. (12) as follows.

$$\left.\begin{aligned}k_1&=1-\frac{u_*}{U}f_0\left(\frac{u_*\delta}{\nu}\right)\cos\beta\\k_2&=-\frac{u_*}{U}f_0\left(\frac{u_*\delta}{\nu}\right)\sin\beta\end{aligned}\right\}\tag{17}$$

Furthermore, velocity profile for the normal velocity component w is necessary to solve the above higher order equations. For simplicity, an approximate profile of w is employed on the basis of the experimental results, although w should be determined to satisfy the continuity equation. Fig. 4 shows the normal velocity component measured near the stern of Ship-A. From these results, the profile of w can approximately be expressed as

$$w=W\cdot\zeta/\delta\tag{18}$$

The normal velocity component W at the boundary layer edge is obtained by integrating the continuity equation. Nakayama et al.[6] and Larsson and Chang[5] are used the same expression of w.

The distribution of turbulent shear stresses in ζ direction is necessary to perform the integral of $\bar{T}_1$ and $\bar{T}_2$ in Eqs. (10) and (11). Referring to turbulence characteristics measured near a ship stern[7], the mixing length l_m is roughly assumed by

$$\left.\begin{aligned}l_m/\delta&=0.2\zeta/\delta\qquad 0\leq\zeta/\delta<0.3\\l_m/\delta&=0.06\qquad 0.3\leq\zeta/\delta\leqq 1.0\end{aligned}\right\}\tag{19}$$

and then shear stresses are evaluated as

$$\frac{\tau_{13}}{\rho}=l_m^2\left|\frac{du}{d\zeta}\right|\frac{du}{d\zeta},\qquad\frac{\tau_{23}}{\rho}=l_m^2\left|\frac{du}{d\zeta}\right|\frac{dv}{d\zeta}\tag{20}$$

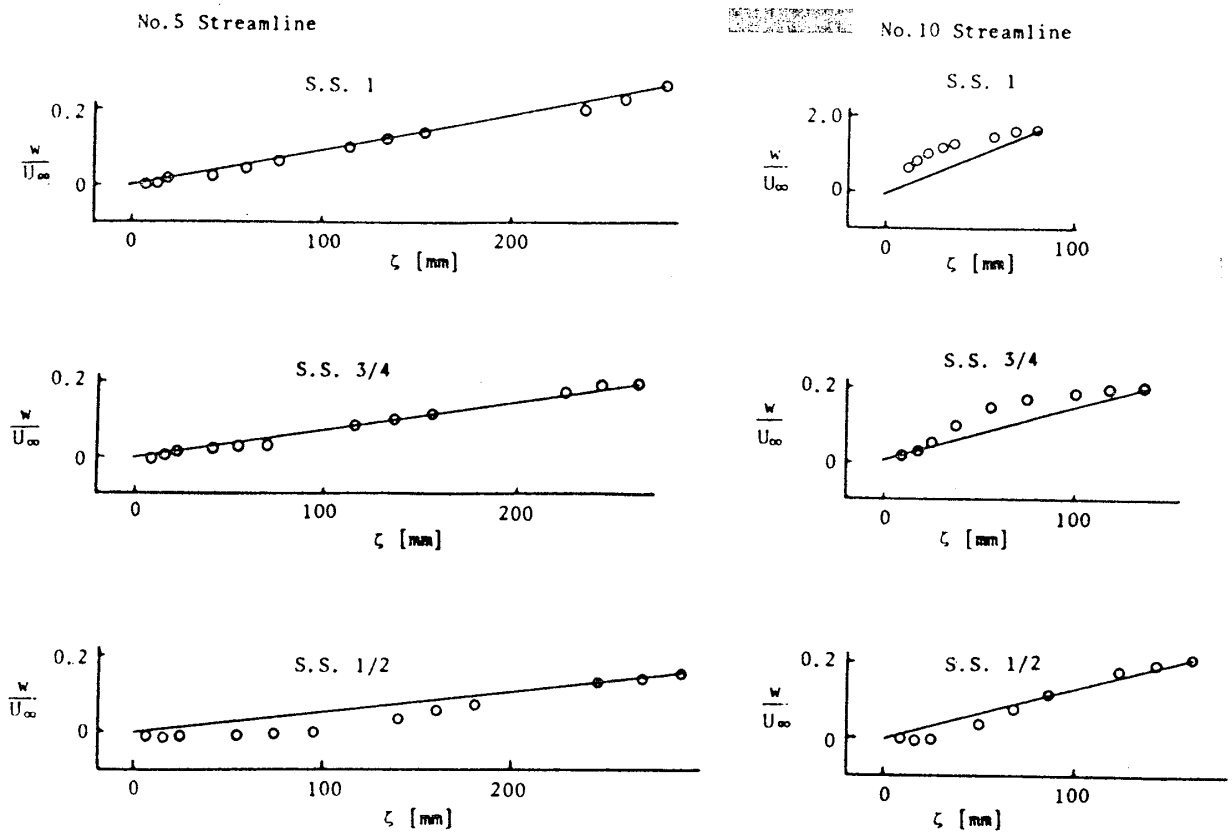

Fig. 4 Measured normal velocity component

An entrainment equation for three-dimensional flow is employed as the auxiliary equation.

$$\frac{1}{h_{1w}}\frac{\partial(\bar{\delta}-\bar{\delta}_1^*)}{\partial\xi}-\frac{1}{h_{2w}}\frac{\partial\bar{\delta}_2^*}{\partial\eta}$$
$$=F-(\bar{\delta}-\bar{\delta}_1^*)\left\{\frac{1}{U}\frac{\partial U}{h_{1w}\partial\xi}+K_{21w}\right\}$$
$$+\bar{\delta}_2^*\left(\frac{1}{U}\frac{\partial U}{h_{2w}\partial\eta}+K_{12w}\right)$$
$$-\frac{W}{U}\{K_{13w}\bar{\delta}+K_{23w}\bar{\delta}\}-\hat{\delta}\frac{\partial K_{23w}}{h_{1w}\partial\xi} \qquad (21)$$

where F is the entrainment rate and Head's relation for two-dimensional flow is applied along the streamline for the three-dimensional flow as

$$\left.\begin{aligned}F&=0.0306(H^*-3.0)^{-0.6153}\\H^*&=(\bar{\delta}-\bar{\delta}_1^*)/\bar{\theta}_{11}\end{aligned}\right\} \qquad (22)$$

2.4 Viscous-inviscid interaction

As mentioned before, the interaction between the boundary layer and the external inviscid flow may become remarkable near the stern, where the flow characteristics are closely related to the viscous pressure resistance.

The viscous-inviscid interaction problem is usually solved by an iterative procedure in which the potential flow and the boundary layer calculations are repeated alternately taking the mutual influence into account. A method adopted in the present paper is the same in the previous paper, and is the so-called surface source method[8),9)]. In the method, the source distribution is determined to allow the specified transpiration velocity on the body surface, resulting from interaction with the boundary layer. The transpiration velocity is determined to satisfy the outer boundary condition which combines smoothly both normal and tangential velocities outside and inside the boundary layer.[3)]

$$W_{pw}=\frac{U}{h_{1w}}\frac{\partial\bar{\delta}_1^*}{\partial\xi}+\frac{U}{h_{2w}}\frac{\partial\bar{\delta}_2^*}{\partial\eta}$$
$$+\bar{\delta}_1^*\left(\frac{\partial U}{h_{1w}\partial\xi}+K_{21w}U\right)$$
$$+\bar{\delta}_2^*\left(\frac{\partial U}{h_{2w}\partial\eta}+K_{12w}U\right)-U\hat{\delta}\frac{\partial K_{23w}}{h_{1w}\partial\xi}$$
$$-\hat{\delta}(K_{23w}+2K_{13w})\left(\frac{\partial U}{h_{1w}\partial\xi}+K_{21w}U\right) \qquad (23)$$

The transpiration velocity W_{pw} tends to increase unreasonably near the stern due to insufficiency of the boundary layer approximation. Following Hoekstra and Raven[10)], an under-relaxation method is adopted for the iterative procedure in the present paper, which is effective to improve the covergence or to avoid divergence.

$$W^{i+1}=W^i+\alpha(W^{i+1}-W^i) \qquad (24)$$

where i is the iteration count and α is the under-

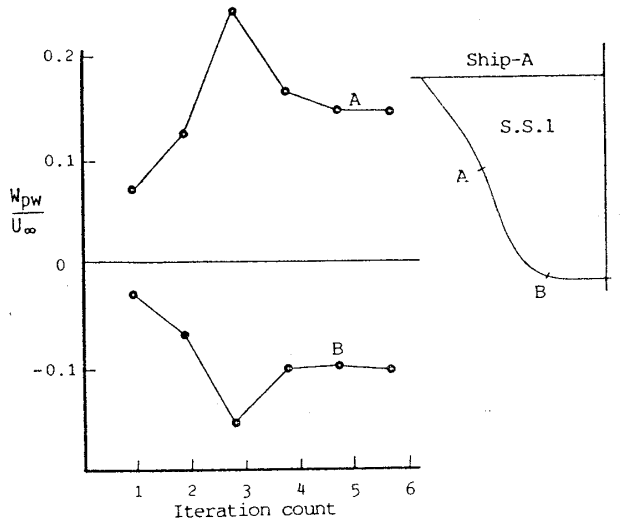

Fig. 5 Transpiration velocity at S.S.1

relaxation factor.

The iterative procedure is terminated when the transpiration velocity W_{pw} attains the value of convergence. As an example, Fig. 5 shows the change of the transpiration velocity at S.S.1 of Ship-A. From the diagram, the iterative procedure may be considered practically to be converged at 6th iteration. It is also found that, at S.S.1, the transpiration velocity is negative on the bottom of ship and positive on the side. This produces extra-sink distributions on the bottom and extra-source distributions on the side at S.S.1 due to the viscous-inviscid interaction. An intensive discussion on the effect of viscous-inviscid interaction is made in Ref. (3).

3. Representation of Ship Hull Form

3.1 Exponential splines

Mathematical expression of hull form is convenient to construct the curvilinear body fitted coordinate system for viscous flow calculations and to change hull form systematically for parametric studies. In this connection, a method proposed by von Kerczeck and Tuck[11] was adopted in the author's previous paper. In the method, each cross section of a ship hull is represented by use of the conformal mapping. The mapping coefficients at each cross section are approximated by polynomials of x. Although this method is simple and expresses a hull form with reasonable accuracy, there are some room for improvements:

(1) Representation of cross sections near aft end is difficult.
(2) The cross sections always intersect with load water line at right angle (recently this is improved by von Kerczeck and Stern[12]).
(3) Undesirable waviness in the longitudinal direction of cross section occurs.
(4) Representation of flat plane such as bottom and vertical wall is impossible.

In the present paper, to improve this situation, exponential splines method is introduced for the expression of hull form.

In general, when x and y are an independent and a dependent variables respectively, and values of y are given at discrete points $x=x_i$, the exponential spline is defined as the solution to the boundary value problem on each subinterval (x_i, x_{i+1}) $(i=1, \cdots, N)$

$$[D^4-p_iD^2]y=0\,, \quad x_i\leq x\leq x_{i+1} \tag{25}$$

and the boundary conditions are

$$y(x_i)=y_i,\ y(x_{i+1})=y_{i+1}\,,$$
$$y''(x_i)=y''_i,\ y''(x_{i+1})=y''_{i+1} \tag{26}$$

where D is differential operator and prim means differential with respect to x. A tention parameter p_i is determined by iterative procedure in order to eliminate extraneous inflection points[13].

If p_i is zero, Eq. (25) becomes a differential equation for a cubic spline and if p_i tends to infinity, the solution of Eq. (25) becomes to be like the polygonal or broken line interpolation.

The general solution of Eq. (25) is written as

$$y=A^*\cosh(p_ix)+B^*\sinh(p_ix)+C^*x+D^* \tag{27}$$

where constants A^*, B^*, C^* and D^* are determined to satisfy the boundary condition (26). This results in

$$y=\frac{1}{p_i^2\sinh(p_ih_i)}\{y''_i\sinh[p_i(x_{i+1}-x)]+y''_{i+1}\sinh[p_i(x-x_i)]\}+\left(y_i-\frac{y''_i}{p_i^2}\right)\frac{x_{i+1}-x}{h_i}+\left(y_{i+1}-\frac{y''_{i+1}}{p_i^2}\right)\frac{x-x_i}{h_i} \tag{28}$$

where

$$h_i=x_{i+1}-x_i \tag{29}$$

The quadratic differential y_i'' $(i=1, \cdots, N+1)$ are determined to satisfy the continuity of first differential at $x=x_i$, and are obtained by solving the following tri-diagonal simultaneous equations.

$$\left(\frac{p_1\cosh(p_1h_1)}{\sinh(p_1h_1)}-\frac{1}{h_1}\right)\frac{y''_1}{p_1^2}+\left(\frac{1}{h_1}-\frac{p_1}{\sinh(p_1h_1)}\right)\frac{y''_2}{p_1^2}=\frac{y_2-y_1}{h_1}-y'_1 \quad \text{for } i=1$$

$$\left(\frac{1}{h_{i-1}}-\frac{p_{i-1}}{\sinh(p_{i-1}h_{i-1})}\right)\frac{y''_{i-1}}{p^2_{i-1}}+\left(\frac{p_{i-1}\cosh(p_{i-1}h_{i-1})}{\sinh(p_{i-1}h_{i-1})}-\frac{1}{h_{i-1}}\right)\frac{1}{p^2_{i-1}}$$

$$\left.\begin{aligned}
&+\left(\frac{p_i\cosh(p_ih_i)}{\sinh(p_ih_i)}-\frac{1}{h_i}\right)\frac{1}{p_i^2}y''_i\\
&+\left(\frac{1}{h_i}+\frac{p_i}{\sinh(p_ih_i)}\right)\frac{y''_{i+1}}{p_i^2}\\
&=\frac{y_{i+1}-y_i}{h_i}-\frac{y_i-y_{i-1}}{h_{i-1}} \qquad \text{for } i=2,\cdots,N\\
&\left(\frac{1}{h_N}-\frac{p_N}{\sinh(p_Nh_N)}\right)\frac{y''_N}{p_N^2}\\
&+\left(\frac{p_N\cosh(p_Nh_N)}{\sinh(p_Nh_N)}-\frac{1}{h_N}\right)\frac{y''_{N+1}}{p_N^2}\\
&=y'_{N+1}-\frac{y_{N+1}-y_N}{h_N} \qquad \text{for } i=N+1
\end{aligned}\right\} \tag{30}$$

3.2 Representation of ship hull form

Now, let us express a hull form by use of the exponential splines. x, y and z are the Cartesian coordinates as shown in Fig. 1, and they are made dimensionless by a half of ship length. A new parameter t is introduced along the frameline at each station and defined as non-dimensional arc length measured from keel line; $t=0$ corresponds to the keel line and $t=1$ to the load waterline. y and z coordinates along frameline at each station are expressed as a function of t by using the exponential splines respectively.

$$y=f(t)\,, \quad z=g(t) \tag{31}$$

Fig. 6 shows a comparison of cross sections of Ship-A expressed by the exponential splines and conformal mapping method. The superiority of the exponential splines can be seen. As frameline expressed by exponential splines coincides completely with one drawn by use of batten, the deviation can not be detected in Fig. 6. Next, s-line is defined longitudinally as a curve of $t=$ constant on the hull surface. y and z coordinates on s-curve are also expressed as a function of x by using the exponential splines.

$$y=F(x)\,, \quad z=G(x) \tag{32}$$

As an example, Fig. 7 shows the body plan and s-curves expressed by the exponential splines. It can be seen that the representation of ship hull form by the exponential splines is satisfactory.

Once Eqs. (31) and (32) are determined for a parent ship form, parametric variations of ship form are easily conducted. For example, a new ship form with different ratio of the principal dimensions is obtained as

$$\left.\begin{aligned}
&y=\gamma_1 f(t)\,, \quad z=\gamma_2 g(t)\\
&y=\gamma_1 F(x)\,, \quad z=\gamma_2 G(x)
\end{aligned}\right\} \tag{33}$$

where γ_1 and γ_2 are constant representing ratios of principal dimensions. Therefore, systematic series of principal dimensions of ship hulls can be constructed immediately by changing the values

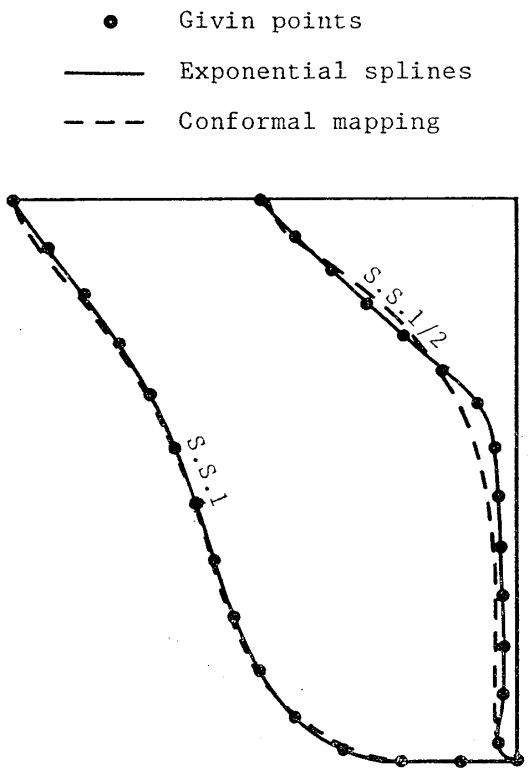

Fig. 6 Comparison of framelines expressed mathematically by two methods

of γ_1 and γ_2. Fig. 8 shows an example: body plan for the values of $\gamma_1=1.0$ and $\gamma_2=1.154$ ($B/d=2.25$) whose parent ship is Ship-A ($B/d=2.6$) shown in Fig. 7. Next, when we want to make minor change of frameline shape locally, only neighbouring framelines and s-lines of the interested part are recalculated to determine their exponential splines. Such a local change of frameline shape is difficult for the conformal mapping method. Further, frameline shape being kept unchanged, parametric changes of sectional area curve and/or fullness of ships may also be possible. It can be therefore said that the present method expressing ship form by exponential splines is satisfactory and useful to investigate on a wide variety of ship forms in the design stage. This method can also be efficiently used in optimization problem by non-linear programming.

4. Calculation of Viscous Resistance

4.1 Method for calculating viscous resistance of ships

Viscous resistance of a ship is obtained as a sum of frictional resistance R_F and viscous pressure resistance R_{vp}. According to their physical properties, R_F can be obtained by integrating the shear stress over the hull surface and R_{vp} by integrating the pressure. Frictional resistance coefficient C_F is expressed as

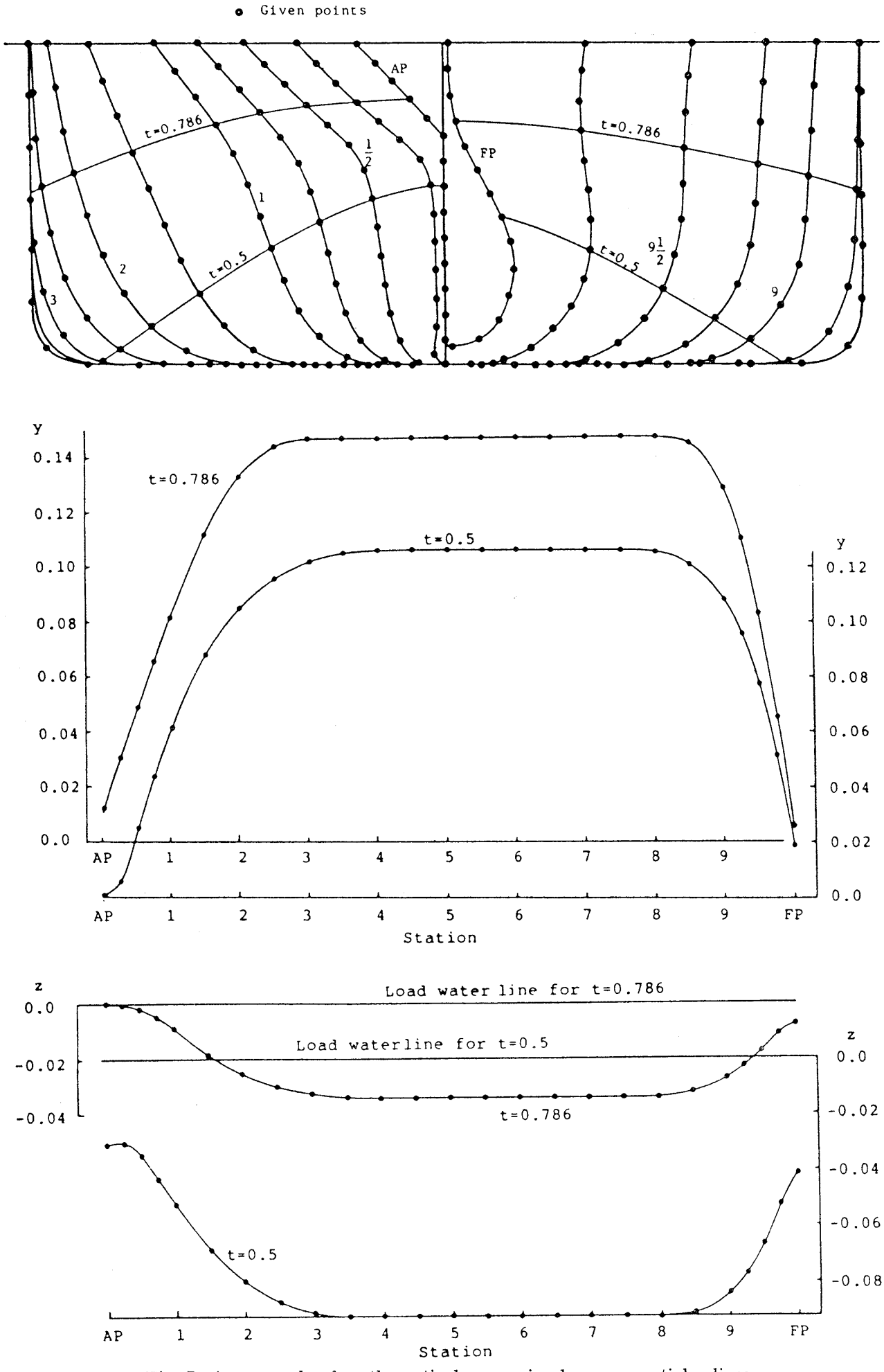

Fig. 7 An example of mathematical expression by exponential splines

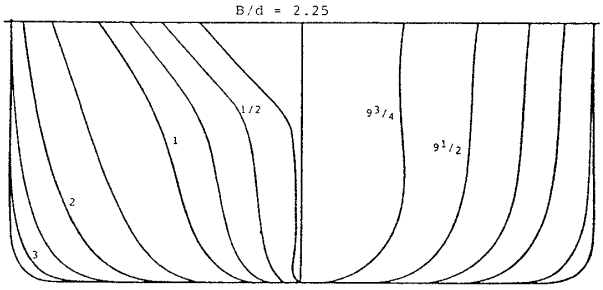

Fig. 8 Body plan of a ship form changed by use of exponential splines

$$C_F=\frac{R_F}{(1/2)\rho U_\infty{}^2 S}=\frac{1}{S}\iint_S \frac{\tau_{wx}}{(1/2)\rho U_\infty{}^2}dS$$
$$=\frac{L_{pp}{}^2}{2S}\left\{\int_{-1}^{x_B} C_F' dx+\int_{x_B}^{1} C_F' dx\right\} \tag{34}$$

where τ_{wx} is x-component of wall shear stress. S and U_∞ are hull surface area and uniform velocity respectively, and x_B denotes the position of numerical breakdown in the boundary layer calculation. C_F' is frictional resistance coefficient at each transverse cross section and is given as

$$C_F'=\int_{-\pi/2}^{0}\frac{\tau_{wx}}{(1/2)\rho U_\infty{}^2}\sigma d\phi \tag{35}$$

where surface element dS is written as

$$dS=\frac{L_{pp}{}^2}{4}\sigma\, dx\, d\phi \tag{36}$$

ϕ is argument when cross section is transformed to the unit circle by conformal mapping.

In the present paper, the second term of the right hand side of Eq. (34) is omitted because its contribution seems to be negligibly small. Viscous pressure resistance coefficient C_{vp} is written as

$$C_{vp}=\frac{R_{vp}}{(1/2)\rho U_\infty{}^2 S}$$
$$=\frac{L_{pp}{}^2}{2S}\left\{\int_{-1}^{x_B} dx\int_{-\pi/2}^{0}(C_{po}-C_{pw})\sigma l\, d\phi\right.$$
$$\left.+\int_{x_B}^{1} dx\int_{-\pi/2}^{0}(C_{po}-C_{pw})\sigma l\, d\phi\right\} \tag{37}$$

where l is x-component of the outward normal unit vector on the hull surface. C_{pw}, C_{pe} and C_{p0} are pressure coefficients defined by

$$\left.\begin{aligned} C_{pw}&=\frac{p_w-p_\infty}{(1/2)\rho U_\infty{}^2},\quad C_{pe}=\frac{p_e-p_\infty}{(1/2)\rho U_\infty{}^2}\\ C_{po}&=\frac{p_o-p_\infty}{(1/2)\rho U_\infty{}^2}\end{aligned}\right\} \tag{38}$$

where p_w and p_0 are the pressure at the hull surface in viscous and potential flows respectively, and p_∞ and p_e represent the reference pressure and the pressure at the boundary layer edge respectively.

In order to understand physical properties of viscous pressure resistance, Eq. (38) is divided into three parts as

$$C_{vp}=C_{vp1}+C_{vp2}+C_{vp3} \tag{39}$$

where

$$\left.\begin{aligned} C_{vp1}&=\frac{L_{pp}{}^2}{2S}\int_{-1}^{x_B} dx\int_{-\pi/2}^{0}(C_{pe}-C_{pw})\sigma l\, d\phi\\ C_{vp2}&=\frac{L_{pp}{}^2}{2S}\int_{-1}^{x_B} dx\int_{-\pi/2}^{0}(C_{po}-C_{pe})\sigma l\, d\phi\\ C_{vp3}&=\frac{L_{pp}{}^2}{2S}\int_{x_B}^{1} dx\int_{-\pi/2}^{0}(C_{po}-C_{pw})\sigma l\, d\phi\end{aligned}\right\} \tag{40}$$

C_{vp1} represents the pressure resistance caused by the pressure variation across the boundary layer and C_{vp2} caused by the viscous-inviscid interaction. C_{vp3} is the pressure resistance at the hull part downstream of the position of numerical breakdown x_B.

An integrand of C_{vp1} can be evaluated by integrating Eq. (8) in ζ direction.

$$C_{pe}-C_{pw}=-2\left(\frac{U}{U_\infty}\right)^2\{\Delta C_{p1}+\Delta C_{p2}+\Delta C_{p3}$$
$$+\Delta C_{p4}+\Delta C_{p5}\} \tag{41}$$

ΔC_{pi} $(i=1,2,3,4,5)$ correspond to the first five terms of Eq. (8) and are given as

$$\left.\begin{aligned} \Delta C_{p1}&=\frac{1}{U^2}\int_0^\delta \frac{\zeta u}{1+K_{13w}\zeta}d\zeta\cdot\frac{1}{h_{1w}}\frac{\partial}{\partial\xi}\left(\frac{W}{\delta}\right)\\ \Delta C_{p2}&=\frac{1}{U^2}\int_0^\delta \frac{\zeta v}{1+K_{23w}\zeta}d\zeta\cdot\frac{1}{h_{2w}}\frac{\partial}{\partial\eta}\left(\frac{W}{\delta}\right)\\ \Delta C_{p3}&=\frac{1}{2}\left(\frac{W}{U}\right)^2\\ \Delta C_{p4}&=-K_{13w}\{(\delta-\delta_1{}^*-\theta_{11})-K_{13w}(\hat{\delta}-\hat{\delta}_1{}^*\\ &\quad-\hat{\theta}_{11})\}\\ \Delta C_{p5}&=K_{23w}(\theta_{22}-K_{23w}\hat{\theta}_{22})\end{aligned}\right\} \tag{42}$$

Using the velocity components U and W at the boundary layer edge, the pressure coefficient C_{pe} at the boundary layer edge is evaluated by

$$C_{pe}=1-(U^2+W^2) \tag{43}$$

As ΔC_{p1}, ΔC_{p2} and ΔC_{p3} depend on the growth of the boundary layer, it may be difficult to know beforehand the correlation between them and geometrical ship form explicitly. On the other hand, ΔC_{p4} and ΔC_{p5} are directly connected to the normal curvatures K_{13w} and K_{23w}. If potential streamline is convex, K_{13w} is positive and then ΔC_{p4} becomes negative. This leads increase of viscous pressure resistance. ΔC_{p5} is usually smaller than ΔC_{p4} because cross flow angles are not so large.

In order to examine accuracy of the present method, the calculated pressure C_{pw} on the hull surface is compared with the measured one in

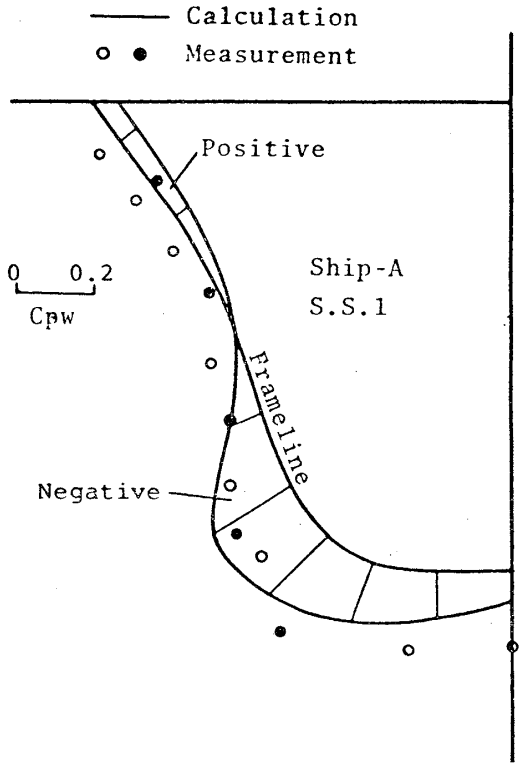

Fig. 9 Comparison of pressure distributions along frameline at S.S.1

Fig. 9. The measurements were made twice on different days for an 8 m long ship model. There is small quantitative gap between calculations and measurements, but a qualitative agreement is fairly well.

Next, let us describe a method to evaluate C_{vp3}. The characteristics of $(C_{p0}-C_{pw})$ values after the position of numerical breakdown were examined on the basis of flow measurements. The pressure C_{pw} on the hull surface of the stern along the four streamlines shown in Fig. 2 was experimentally obtained first and then they are compared with the pressure C_{p0} on the hull surface in the potential flow in Fig. 10. It is noticed that the difference between C_{p0} and C_{pw} increases gradually towards the stern end. The same is observed in other experiments by, for example, Larsson[14] and Hatano et al.[15] However, an increment of the difference is very small, therefore it may be assumed that the difference between C_{p0} and C_{pw} is constant along the streamlines, viz.

$$C_{vp3}=\frac{L_{pp}^2}{2S}\iint_{x_B}(C_{p0}-C_{pw})\,dy\,dz \qquad (44)$$

const. along each streamline

4.2 Calculated results and discussion

The viscous resistance coefficients of Ship-A are calculated by the method described above and are shown in Table 1. In the case of Ship-A, C_{vp1}, C_{vp2} and C_{vp3} are almost same magnitude, though C_{vp2} is negative value.

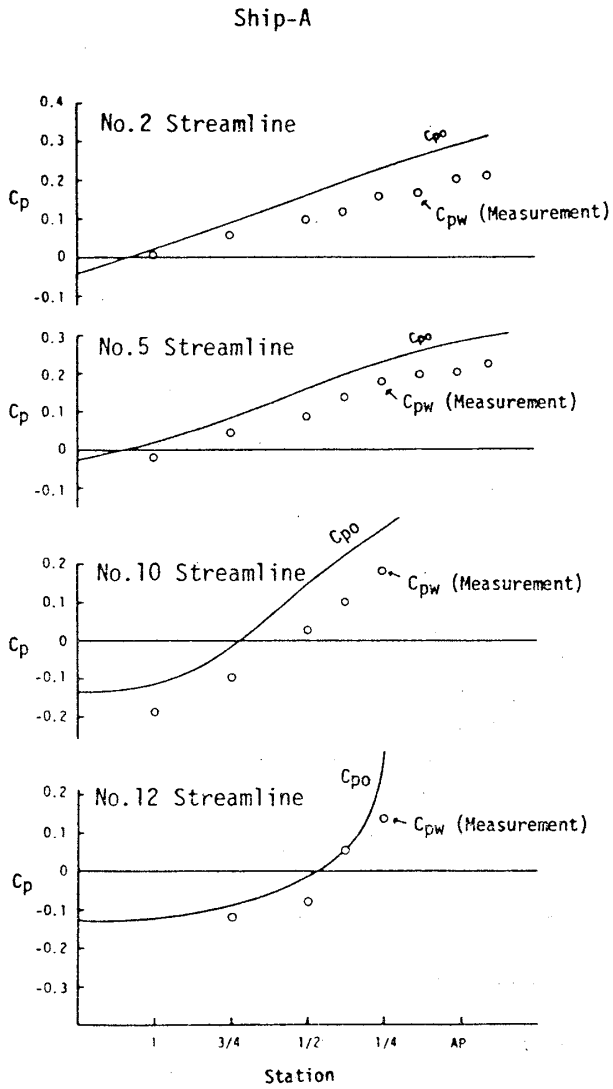

Fig. 10 Pressure distributions measured near the stern

C_{F0}, the frictional resistance coefficient for a flat plate, is calculated by applying the present method, and form factor K_f due to the frictional resistance and K_p due to the viscous pressure resistance are calculated by

$$1+K_f=C_F/C_{F0}\,,\quad K_p=C_{vp}/C_{F0} \qquad (45)$$

K_p is considerably larger than K_f as can be seen in Table 1. Therefore, it is said that much attention should be paid to the viscous pressure resistance in the design of full form ships. The calculated form factor K is slightly smaller than the experimental one Kexp obtained from the resistance test. However, the degree of this discrepancy seems to be acceptable in practical use.

Next, viscous resistance calculations were performed for full form ships whose breadth-draught ratio was changed by use of aforementioned exponential splines. Body plan of the ship

Table 1 Principal dimensions and calculated results of viscous resistance

Items		Ship-A Original	Ship-A B/d series		Ship-B U-form	Ship-C V-form
Lpp (m)		8.00	8.00	8.00	5.00	5.00
Lpp/B		6.83	6.83	6.83	6.00	6.00
B/d		2.60	2.25	3.00	2.76	2.76
Cb		0.83	0.83	0.83	0.80	0.80
Rn x 10^{-6}		12.2	12.2	12.2	5.0	5.0
C_{F0}		0.00269	0.00269	0.00269	0.00308	0.00308
Kexp		0.322	-----	-----	0.425	0.358
Calculation	Cvp1	0.00056	0.00066	0.00103	0.00043	0.00086
	Cvp2	-0.00050	-0.00079	-0.00090	-0.00021	-0.00059
	Cvp3	0.00044	0.00098	0.00035	0.00128	0.00070
	C_F	0.00293	0.00295	0.00291	0.00332	0.00340
	Kp	0.186	0.316	0.178	0.487	0.313
	K_f	0.089	0.097	0.082	0.078	0.104
	K	0.275	0.413	0.260	0.565	0.417
	Cvcal/Cvexp	0.964	-----	-----	1.098	1.043

Note; $Cvcal = Cvp + C_F$, $Cvexp = C_{F0}(1+Kexp)$

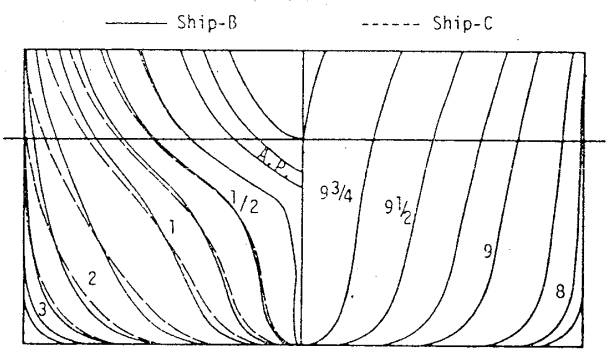

Fig. 11 Body plans of two tanker models

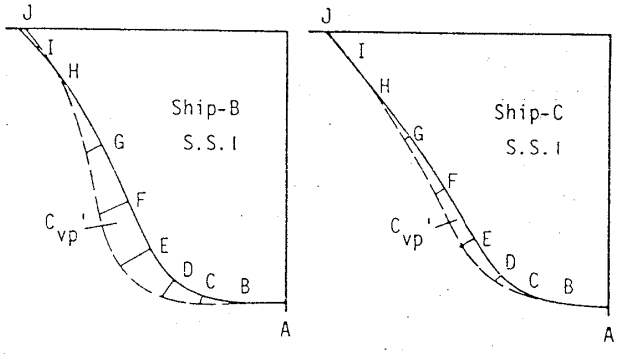

Fig. 12 Distributions of viscous pressure resistance component at S.S.1

with breadth-draught ratio of 2.25 is shown in Fig. 8. According to the calculated results shown in Table 1, the viscous resistance of the ship with smaller B/d is larger than that with larger B/d. This trend agrees with the experimental results[1]. It is also found that the difference of viscous resistance among them comes from the difference of the viscous pressure resistance, because frictional resistance is almost same.

Lastly, viscous resistance calculated and measured for two tanker models[16], Ship-B and Ship-C, are shown in Table 1. Their fore-bodies are identical and the shape of frameline of their after-bodies are slightly different as shown in Fig. 11. The calculated results agree with the measured ones fairly well and the present method detects the difference of viscous resistance caused from small difference of frameline shapes as well as measurements. Fig. 12 shows the girthwise distributions of viscous pressure resistance component calculated at S.S.1. An evident difference between Ship-B and Ship-C is observed along the girth from position C to G. The viscous pressure resistance is obtained by multipling the

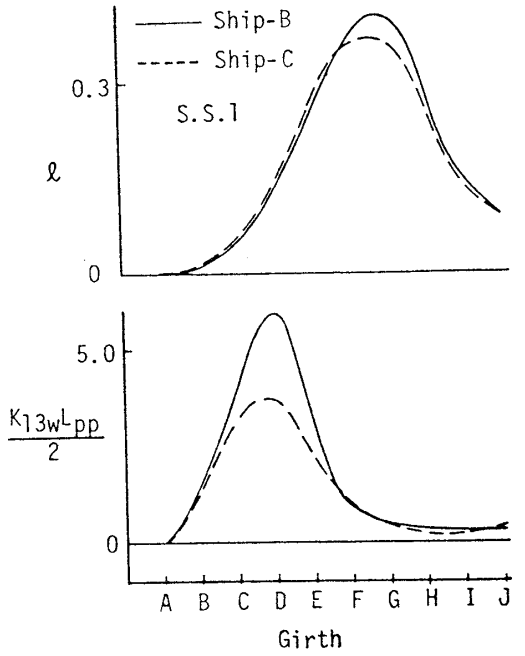

Fig. 13 Comparison of directional cosine and normal curvature

directional cosine l at the hull surface to $(C_{p0}-C_{pw})$, and the normal curvatures K_{13w} and K_{23w} are closely connected to $(C_{p0}-C_{pw})$ as known from Eq. (42). Consequently, directional cosine l and normal curvatures, especially K_{13w}, are important geometrical quantities. The girthwise distributions of l and K_{13w} at S.S.1 of both ship models are compared in Fig. 13. A considerable difference of K_{13w} is observed between positions C and E, while l is almost same magnitude in both models. This implies that larger viscous pressure resistance component of Ship-B shown in Fig. 12 is mainly caused from larger normal curvature K_{13w}.

As described above, the present calculation method can predict viscous resistance of full form ships and understand the relationship between the viscous pressure resistance and local hull form. Therefore, the present method may become a useful tool for design and improvement of hull form.

5. Concluding Remarks

An improved method for calculating ship viscous resistance is presented. The viscous resistance is calculated as a sum of frictional and viscous pressure resistance, which are obtained by integrating shear stress and pressure over the hull surface in order to know directly the correlation between the hull form and viscous resistance components. The shear stress and pressure on the hull surface are obtained by solving the momentum integral equations of the boundary layer, including higher order terms and viscous-inviscid interaction which characterize thick boundary layer near the stern.

Furthermore, in order to make systematic changes of ship form easily and to examine many candidates of the ship on their viscous resistance quickly and cheaply at the design stage, ship form is represented mathematically by use of the exponential splines. It is found that this method representing hull form is satisfactory and effective for practical use.

The calculated results of viscous resistance of full form ships by the present method agree well with the measured ones. And then it is expected that the present method including mathematical representation of hull forms may become a useful tool for designing ship hull forms.

Acknowledgement

The author wishes to express his heartly appreciation to Professor R. Yamazaki, Kyushu University, for his kind encouragement and guidance of the present study. He also wishes to express his sincere gratitude to Dr. E. Baba, Project Manager of Ship Hydrodynamics Research Laboratory, Nagasaki Technical Institute, MHI, for his continuing guidance and valuable discussion. Thanks are also extended to all the members of the Nagasaki Experimental Tank for their cooperation.

References

1) Nagamatsu, T., Sakamoto, T. and Baba, E.: Study on the Minimization of Ship Viscous Resistance, Journal of the Society of Naval Architects of Japan, Vol. 154, 1983.
2) Nagamatsu, T.: Calculation of Viscous Pressure Resistance of Ships Based on a Higher Order Boundary Layer Theory, Journal of the Society of Naval Architects of Japan, Vol. 147, 1980.
3) Nagamatsu, T.: Calculation of Ship Viscous Resistance by Integral Method and Its Application, 2nd International Symposium on Ship Viscous Resistance, Göteborg, 1985.
4) SR107: Investigation into the Speed Measurement and Improvement of Accuracy in Powering of Full Ships, The Shipbuilding Research Association of Japan, Report No. 73, 1973.
5) Larsson, L. and Chang, M-S.: Numerical Viscous and Wave Resistance Calculations Including Interaction, 13th Symposium on Naval Hydrodynamics, Tokyo, 1980.
6) Nakayama, A., Patel, V. C. and Landweber, L.: Flow Interaction Near the Tail of a

Body of Revolution, Journal of Fluids Engineering, Transactions of ASME, Series I, Vol. 98, No. 3, 1976.

7) Hatano, S. and Hotta, T.: Turbulence Measurements in the Flow Around a Body in a Circulating Water Channel (Part 2). Transactions of the West-Japan Society of Naval Architects, No. 64, 1982.

8) Lighthill, M. J.: On the Displacement Thickness, Journal of Fluid Mechanics, Vol. 4, 1958.

9) Himeno, Y. and Okuno, T.: Pressure Distribution in Ship Boundary Layer and Its Displacement Effect, Journal of the Kansai Society of Naval Architects, Japan, No. 174, 1979.

10) Hoekstra, M. and Raven, H. C.: Calculation of Viscous-Inviscid Interaction in the Flow Past a Ship Afterbody, 13th Symposium on Naval Hydrodynamics, Tokyo, 1980.

11) von Kerczek, C. and Tuck, E. O.: The Representation of Ship Hulls by Conformal Mapping Functions, Journal of Ship Research, Vol. 13, 1969.

12) von Kerczek, C. and Stern, F.: The Representation of Ship Hulls by Conformal Mapping Functions: Fractional Maps, Journal of Ship Research, Vol. 27, No. 3, 1983.

13) McCartin, B. J.: Applications of Exponential Splines in Computational Fluid Dynamics, AIAA Journal, Vol. 21, No. 8, 1983.

14) Larsson, L.: Boundary Layers of Ships. Part III: An Experimental Investigation of the Turbulent Boundary Layer on a Ship Model, Report No. 46 of the Swedish Maritime Research Center SSPA. 1974.

15) Hatano, S., Mori, K. and Hotta, T.: Experimental and Theoretical Investigation of Ship Boundary Layer and Wake, 12th Symposium on Naval Hydrodynamics, Washington, D. C., 1978.

16) SR159, The Shipbuilding Research Association of Japan, 1977.

Appendix Definition of integral parameters

$$U^2\theta_{11}=\int_0^\delta u(U-u)d\zeta\,,\qquad U^2\hat{\theta}_{11}=\int_0^\delta \zeta u(U-u)d\zeta$$

$$U^2\theta_{12}=\int_0^\delta v(U-u)d\zeta\,,\qquad U^2\hat{\theta}_{12}=\int_0^\delta \zeta v(U-u)d\zeta$$

$$U^2\theta_{21}=-\int_0^\delta uv\,d\zeta\,,\qquad U^2\hat{\theta}_{21}=-\int_0^\delta \zeta uv\,d\zeta$$

$$U^2\theta_{22}=-\int_0^\delta v^2 d\zeta\,,\qquad U^2\hat{\theta}_{22}=-\int_0^\delta \zeta v^2\,d\zeta$$

$$U^2\theta_{13}=\int_0^\delta w(U-u)d\zeta\,,\qquad U^2\hat{\theta}_{13}=\int_0^\delta \zeta w(U-u)d\zeta$$

$$U^2\theta_{23}=-\int_0^\delta vw\,d\zeta\,,\qquad U^2\hat{\theta}_{23}=-\int_0^\delta \zeta vw\,d\zeta$$

$$U^2\theta_{31}=\int_0^\delta u(W-w)d\zeta\,,\qquad U^2\hat{\theta}_{31}=\int_0^\delta \zeta u(W-w)d\zeta$$

$$U\delta_1^*=\int_0^\delta (U-u)d\zeta\,,\qquad U\hat{\delta}_1^*=\int_0^\delta \zeta(U-u)d\zeta$$

$$U\delta_2^*=-\int_0^\delta v\,d\zeta\,,\qquad U\hat{\delta}_2^*=-\int_0^\delta \zeta v\,d\zeta$$

$$U^2I_1=\int_0^\delta d\zeta\int_\zeta^\delta \frac{u^2}{(1+K_{13w}\zeta)}\,d\zeta$$

$$U^2\hat{I}_1=\int_0^\delta \zeta\,d\zeta\int_\zeta^\delta \frac{u^2}{(1+K_{13w}\zeta)}\,d\zeta$$

$$U^2I_2=\int_0^\delta d\zeta\int_\zeta^\delta \frac{v^2}{(1+K_{23w}\zeta)}\,d\zeta$$

$$U^2\hat{I}_2=\int_0^\delta \zeta\,d\zeta\int_\zeta^\delta \frac{v^2}{(1+K_{23w}\zeta)}\,d\zeta$$

$$U^2I_3=\int_0^\delta J d\zeta\,,\qquad U^2\hat{I}_3=\int_0^\delta \zeta J\,d\zeta$$

$$J=\int_\zeta^\delta\left(\frac{u}{h_1}\frac{\partial w}{\partial\xi}+\frac{v}{h_2}\frac{\partial w}{\partial\eta}+w\frac{\partial w}{\partial\zeta}\right)d\zeta$$

$$T_1=\int_0^\delta \frac{\tau_{13}}{\rho U^2}d\zeta\,,\qquad \hat{T}_1=\int_0^\delta \zeta\frac{\tau_{13}}{\rho U^2}d\zeta$$

$$T_2=\int_0^\delta \frac{\tau_{23}}{\rho U^2}d\zeta\,,\qquad \hat{T}_2=\int_0^\delta \zeta\frac{\tau_{23}}{\rho U^2}d\zeta$$

and

$$\tilde{\theta}_{11}=\theta_{11}+K_{13w}\hat{\theta}_{11}$$

$$\tilde{\theta}_{11}=\theta_{11}+K_{23w}\hat{\theta}_{11}\,,\qquad \tilde{\theta}_{12}=\theta_{12}+K_{13w}\hat{\theta}_{12}$$

$$\tilde{\theta}_{21}=\theta_{21}+K_{23w}\hat{\theta}_{21}\,,\qquad \tilde{\theta}_{21}=\theta_{21}+K_{13w}\hat{\theta}_{21}$$

$$\tilde{\theta}_{22}=\theta_{22}+K_{23w}\hat{\theta}_{22}\,,\qquad \tilde{\theta}_{22}=\theta_{22}+K_{13w}\hat{\theta}_{22}$$

$$\tilde{\theta}_{13}=\theta_{13}+K_{23w}\hat{\theta}_{13}\,,\qquad \tilde{\theta}_{13}=\theta_{13}+K_{13w}\hat{\theta}_{13}$$

$$\tilde{\theta}_{23}=\theta_{23}+K_{23w}\hat{\theta}_{23}\,,\qquad \tilde{\theta}_{23}=\theta_{23}+K_{13w}\hat{\theta}_{23}$$

$$\tilde{\theta}_{31}=\theta_{31}+K_{23w}\hat{\theta}_{31}\,,\qquad \tilde{\theta}_{31}=\theta_{31}+K_{13w}\hat{\theta}_{31}$$

$$\tilde{\delta}_1^*=\delta_1^*+K_{23w}\hat{\delta}_1^*\,,\qquad \tilde{\delta}_2^*=\delta_2^*+K_{13w}\hat{\delta}_2^*$$

$$\tilde{\delta}=\delta+K_{23w}\hat{\delta}\,,\qquad \tilde{\delta}=\delta+K_{13w}\hat{\delta}$$

$$\tilde{I}_1=I_2+K_{23w}\hat{I}_1\,,\qquad \tilde{I}_1=I_1+K_{13w}\hat{I}_1$$

$$\tilde{I}_2=I_2+K_{23w}\hat{I}_2\,,\qquad \tilde{I}_2=I_2+K_{13w}\hat{I}_2$$

$$\tilde{I}_3=I_3+K_{23w}\hat{I}_3\,,\qquad \tilde{I}_3=I_3+K_{13w}\hat{I}_3$$

$$\tilde{T}_1=T_1+K_{23w}\hat{T}_1\,,\qquad \tilde{T}_2=T_2+K_{13w}\hat{T}_2$$

where δ is the boundary layer thickness and

$$\hat{\delta}=\frac{1}{2}\delta^2$$

τ_{13w} and τ_{23w} are the wall shear stresses in ξ and η directions.